Transit Timing of the White Dwarf-Cold Jupiter System WD 1856+534

ELI A. GENDREAU-DISTLER , ¹ KATE B. BOSTOW , ^{1,2} KISHORE C. PATRA , ^{1,3} EFRAIN ALVARADO III , ^{1,2} ANDREAS BETZ, ¹ VICTORIA M. BRENDEL, ¹ VIDHI CHANDER, ¹ ASIA A. DEGRAW, ¹ COOPER JACOBUS , ¹ CONNOR F. JENNINGS, ¹ ANN MINA, ¹ ANSEL PARKE, ¹ RILEY PATLAK, ¹ NEIL R. PICHAY, ¹ SOPHIA RISIN, ¹ EDGAR P. VIDAL , ^{1,4} WILLIAM WU, ¹ THOMAS G. BRINK , ¹ WEIKANG ZHENG , ¹ AND ALEXEI V. FILIPPENKO , ¹

¹Department of Astronomy, University of California, Berkeley, CA 94720-3411, USA
 ²Department of Physics & Astronomy, San Francisco State University, 1600 Holloway Avenue, San Francisco, CA 94132, USA
 ³Department of Astronomy & Astrophysics, University of California, Santa Cruz, CA 95064, USA
 ⁴Department of Physics & Astronomy, Tufts University, Medford, MA 02155, USA

ABSTRACT

We present new transit timing measurements for the white dwarf-cold Jupiter system WD 1856+534, extending the baseline of observations from 311 epochs to 1498 epochs. The planet is unlikely to have survived the host star's red-giant phase at its present location and is likely too small for commonenvelope evolution to take place. As such, a plausible explanation for the short semimajor axis is that the exoplanet started out on a much larger orbit and then spiraled inward through high-eccentricity tidal migration (HETM). A past transit-timing analysis found tentative evidence for orbital growth, which could have been interpreted as a residual effect of HETM, but we find the data are consistent with a constant-period model after adding 18 new transit measurements. We use the estimated period derivative $\dot{P} = 0.04 \pm 0.43$ ms yr⁻¹ to place a lower limit on the planetary tidal quality factor of $Q_n \ge 3.1 \times 10^6$, consistent with that of Jupiter in our own Solar System. We also test for the presence of companion planets in the system, which could have excited WD 1856 b onto an eccentric orbit via the Kozai-Lidov process, and ultimately rule out the presence of an additional planet with a mass greater than $4.1 M_J$ and a period shorter than 1500 days. We find no evidence for nonzero eccentricity, with an upper limit of $e \le 10^{-2}$. If the planet indeed reached its current orbit through HETM, the low present-day eccentricity indicates that the migration process has now ceased, and any further orbital evolution will be governed solely by weak planetary tides.

Keywords: Exoplanets (498) — Exoplanet migration (2205) — White dwarf stars (1799) — Star-planet interactions (2177) — Transit photometry (1709) — Transit timing variation method (1710)

1. INTRODUCTION

Most stars in our Galaxy host exoplanet systems and will eventually evolve into white dwarfs, yet only a handful of exoplanets orbiting white dwarfs have been detected to date (see, e.g., Thorsett et al. 1993; Luhman et al. 2011; Gänsicke et al. 2019; Vanderburg et al. 2020; Blackman et al. 2021; Veras 2021; Zhang et al. 2024). Such systems offer a unique glimpse of what the future might hold for the nearly 6000 known planets around low-mass main-sequence stars. Many close-in planets are expected to be engulfed by the red-giant phase of the host star — and indeed, recently, an exoplanet was

Email: egendreaudistler@berkeley.edu, kcpatra@ucsc.edu

observed being engulfed by its Sun-like host star (De et al. 2023) — but some may survive. At present, many questions remain unanswered about how planets that avoid engulfment will be affected by their host star's post-main-sequence evolution. For example, it is unclear how a planet could end up on an orbit so tight that it should have been consumed during the host star's redgiant phase (Villaver & Livio 2009; Mustill & Villaver 2012; Maldonado et al. 2020). Characterizing the orbital properties of exoplanets around white dwarfs promises to advance our understanding of planetary migration while also helping to constrain the tidal properties of white dwarfs.

A quarter century elapsed between the discovery of the first exoplanet orbiting a main-sequence star (Mayor

& Queloz 1995) and the discovery of the first closein exoplanet orbiting a white dwarf (Vanderburg et al. 2020). In the interim, indirect evidence for the existence of planetary systems around white dwarfs continued to accumulate through observations of metal pollution in white-dwarf atmospheres (e.g., Zuckerman et al. 2010; Debes et al. 2012; Koester et al. 2012, 2014; Wilson et al. 2014; Raddi et al. 2015; Hollands et al. 2017; Blouin et al. 2019; Preval et al. 2019) and of debris and gas disks around polluted white dwarfs (e.g., Kilic et al. 2005, 2006; Kilic & Redfield 2007; Kilic et al. 2012; Gänsicke et al. 2006; Brinkworth et al. 2009, 2012; Barber et al. 2012; Farihi et al. 2016; Hartmann et al. 2016). These observations were further reinforced by the detections of a circumbinary planet orbiting the whitedwarf-pulsar system PSR B1620-26 (Sigurdsson et al. 2003), an extremely distant companion to WD 0806-661 (Luhman et al. 2011), a disintegrating planetesimal transiting WD 1145+017 (Vanderburg et al. 2015), and an evaporating giant planet orbiting WD J0914+1914 (Gänsicke et al. 2019). However, it was not until 2020 that Vanderburg et al. (2020) announced the discovery of WD 1856+534b, the first intact exoplanet detected on a close-in orbit around a white dwarf.

WD 1856+534 b is a Jupiter-sized planet orbiting the white dwarf WD 1856+534 (hereafter WD 1856) at an orbital distance of merely 0.0204 AU (Vanderburg et al. 2020). Unlike most transits of close-in giant planets — which reach a transit depth of at most a few percent over an hours-long transit — the (grazing) WD 1856 b transit reaches a 56% depth in a short 8 min transit. The short transit duration is typical of exoplanets around white dwarfs owing to the small R_* of the star, and the large transit depth is a result of the high planet-to-star radius ratio $R_p/R_* = 7.28$ (Vanderburg et al. 2020).

The WD 1856 system has sparked considerable interest in the exoplanet community because the cold Jupiter lies in the host star's "forbidden zone," meaning that it should not have survived the red-giant phase at its present location (Limbach et al. 2025). Many hypotheses have been proposed to explain how the planet ended up on such a tight orbit through either commonenvelope evolution (Lagos et al. 2020; Vanderburg et al. 2020; Chamandy et al. 2021; Merlov et al. 2021; Xu et al. 2021) or high-eccentricity tidal migration (HETM; Vanderburg et al. 2020; O'Connor et al. 2020; Stephan et al. 2021; Maldonado et al. 2020; Muñoz & Petrovich 2020). Under common-envelope evolution, the planet is engulfed by the expanding star's envelope and begins to spiral inward as it loses orbital energy to drag and friction within the envelope. The release of orbital energy can, in some cases, be sufficient to unbind and

eject the common envelope, leaving behind an intact planet on a close-in orbit (Ivanova et al. 2020). This mechanism is most frequently invoked to explain close binary stars, but it could also apply to the WD 1856 system if the planet is sufficiently massive and if an additional energy source, besides gravitational potential energy, helps to eject the envelope (Lagos et al. 2020; Vanderburg et al. 2020; Merlov et al. 2021). However, recent James Webb Space Telescope (JWST) observations targeting the WD 1856 system have confirmed that the planet mass is at most $6\,M_J$, which is likely too small to successfully expel the envelope (Limbach et al. 2025).

Alternatively, it is possible that WD 1856 b survived the red-giant phase at a larger orbital distance and was brought to its present close-in orbit via tidal circularization. In order for tidal circularization to take place, the planet would first need to be excited onto a highly eccentric orbit through interactions with other bodies within or near the system. One way this could happen is through the Kozai-Lidov mechanism, in which the exchange of angular momentum between bodies in the system leads to periodic oscillations in the orbital eccentricity and inclination (Kozai 1962; Lidov 1962; Naoz 2016). Prior studies have proposed that this initial excitation could have been caused by interactions with the M-dwarfs G229-20A/B (which form a triplestar system with WD 1856), a stellar flyby, or additional planets in the WD 1856 system (Vanderburg et al. 2020; O'Connor et al. 2020; Stephan et al. 2021; Maldonado et al. 2020). After being excited onto a sufficiently eccentric orbit (Muñoz & Petrovich 2020; O'Connor et al. 2020), WD 1856 b would have lost energy to the white dwarf owing to tidal dissipation at periapse, which would ultimately lead to a tight circular orbit as we observe today (Dawson & Johnson 2018). Detecting or ruling out the presence of additional planets and residual eccentricity in the system will help us understand whether high-eccentricity tidal migration is a probable explanation for WD 1856 b's remarkably tight orbit.

In addition to distinguishing between possible formation mechanisms, transit timing of WD 1856 b can also shed light on the tidal properties of the two bodies in the system. Currently, there are only two exoplanets confirmed to be undergoing orbital decay: WASP-12 b (Patra et al. 2017; Yee et al. 2020) and Kepler-1658 b (Vissapragada et al. 2022). Long-term transit-timing measurements of these two systems enabled astronomers to place new constraints on the stellar tidal quality factor, an important property describing the efficiency of tidal dissipation in the host star. The modified stellar tidal quality factor Q'_* of white dwarfs remains poorly constrained because their degenerate, highly compact inter-

nal structure makes the tidal dissipation extremely small and thus difficult to measure (Becker et al. 2023). Studies of inspiraling C-O white-dwarf binaries have placed $Q'_* \approx 10^7$ (Piro 2011; Burkart et al. 2013). A direct measurement of Q'_* for an isolated white dwarf is currently lacking but is expected to lie in the range 10^{12} – 10^{15} (Willems et al. 2010; Becker et al. 2023). If the WD 1856 system were undergoing orbital decay or orbital growth, then we would be able to constrain the tidal properties of the white dwarf based on the observed rate of change of the period. Alternatively, if Q'_* is found to be consistent with infinity, then we can interpret the evolution of the system as being driven by tides raised on the planet and can thus constrain the planetary tidal quality factor Q'_{p} . Jupiter-sized exoplanets are expected to have tidal properties similar to those of our own Jupiter, but there are few tight constraints on the tidal quality factor for planets outside our Solar System to date (see, e.g., Efroimsky & Makarov 2022; Fellay, L. et al. 2023; Louden et al. 2023).

Recent advances in direct imaging and microlensing have enabled further progress in the study of exoplanetary systems around white dwarfs. In 2024, JWST directly imaged giant-planet candidates orbiting white dwarfs WD 1202-232 and WD 2105-82 (Mullally et al. 2024). In addition, the microlensing event KMT-2020-BLG-0414 has been interpreted as a lens system consisting of a white dwarf orbited by an Earth-mass planet and a brown dwarf (Zhang et al. 2024). Transmission spectroscopy is another area with huge potential for advancing our understanding of planetary systems around white dwarfs, particularly because of the high planetto-star radius ratio (Kaltenegger et al. 2020). Indeed, Xu et al. (2021) and Alonso et al. (2021) constrained WD 1856 b's mass to be greater than $0.84 M_J$ and $2.4\,M_{J}$ (respectively) using transmission spectroscopy, and these constraints are likely to improve with additional JWST data. As more exoplanets are detected around white dwarfs, it becomes increasingly important to understand how these systems form and evolve through their host stars' post-main-sequence evolution. The WD 1856 system presents a unique opportunity to do exactly that because the planet's orbit is not easily explained by any of the leading formation hypotheses.

The goal of this paper is to extend the transit-timing baseline of WD 1856 b in order to place tighter constraints on the system's tidal quality factor and on additional planets in the system. The remainder of the paper is organized as follows. Section 2 describes our procedures for collecting, reducing, and analyzing the new transit light curves. Section 3 outlines our approach to deriving constraints on the planetary tidal quality factor

and on additional planets from transit-timing variations (TTVs). We discuss our results in Section 4 and summarize our conclusions in Section 5.

2. METHODS

2.1. Observations

We observed 20 transits of WD 1856 b on the 1 m Nickel telescope at Lick Observatory atop Mount Hamilton, California. The Nickel Direct Imaging Camera is a Loral 2048 × 2048 pixel CCD with an approximately $6.3' \times 6.3'$ field of view. Most transits were observed with 45 s exposures in the Bessel R filter. The filter was selected based on the white dwarf's effective temperature of 4710 K (reported by Vanderburg et al. 2020), and the exposure time was selected so as to maximize the signal-to-noise ratio while maintaining a high cadence of observations to sufficiently sample the ~ 8 min transit. The only exceptions were the 2022 April 2 transit, which was observed in the Bessel V filter with 45 s exposures, and the 2022 June 3 transit, which was observed in the Bessel V filter with 45 s exposures.

2.2. Data reduction

We carried out bias subtraction and flat-field division using AstroImageJ (AIJ), an image-processing package specialized for calibrating and reducing astronomical datasets (Collins et al. 2017). We also used AIJ to perform aperture photometry on the target star and four nearby comparison stars of similar brightness. The aperture size was chosen automatically based on the full width at half-maximum intensity (FWHM): typically around 10 pixels for the photometric aperture, 18 pixels for the inner background annulus, and 28 pixels for the outer background annulus. We defined the relative flux to be the ratio of the target star's flux to the sum of the comparison stars' fluxes. This relative flux was normalized to unity outside the transit. The time stamp associated with each image was taken to be the Barycentric Julian Date in Barycentric Dynamical Time (BJD_{TDB}) corresponding to the mid-exposure.

2.3. Light curves

Using the Mandel & Agol (2002) transit model, we parameterized each transit light curve by the mid-transit time $(T_{\rm mid})$, scaled stellar radius (R_*/a) , planet-to-star radius ratio (R_p/R_*) , and impact parameter $(b=a\cos i/R_*)$. Though atmospheric extinction is relatively constant over the short 8 min transit, it can have a noticeable effect across the out-of-transit baselines on either side of the transit; as such, we introduced two additional free parameters to model the relative flux as a linear function of time. We also included a nuisance pa-

rameter $\log f$ to account for possible mismodeling of the uncertainties.

The effect of limb darkening is challenging to model because the WD 1856 b transit is grazing, which means that we may not sample the full limb-darkening profile of the stellar disk over the duration of the transit (Xu et al. 2021). Moreover, our individual transit light curves are too sparsely sampled to fit the limb-darkening coefficients as free parameters before stacking the light curves. To work around this, we took an iterative approach in which the mid-transit times are first estimated by fitting the individual light curves with tabulated limb-darkening coefficients; these mid-transit times are then used to stack the transit observations in order to produce a well-sampled light curve which can be fit with the limb-darkening coefficients as free parameters.

More specifically, we performed a preliminary fit on the individual light curves assuming a quadratic limbdarkening law with the limb-darkening coefficients reported by Eastman et al. (2013). When calculating these coefficients we adopted the effective temperature, $T_{\rm eff} = 4710 \, \mathrm{K}$, and surface gravity, $\log g = 7.915$, reported by Vanderburg et al. (2020), and the lowest metallicity included in the tables, [Fe/H] = -4.5. We specified uniform priors for all seven free parameters and used the emcee Markov chain Monte Carlo (MCMC) ensemble sampler to approximate the posterior distributions (Foreman-Mackey et al. 2013). All MCMC fits were performed with 32 walkers initialized around the maximum-likelihood solution obtained from SciPy's numerical optimizer (Virtanen et al. 2020). We then subtracted the optimal mid-transit time from the time stamps in the individual light curves and combined the resulting data points across all transits to obtain the stacked light curve shown in Figure 1. To better constrain the physical parameters, we fit another Mandel & Agol (2002) model to the stacked light curve with the limb-darkening parameters treated as free parameters (see Table 1). Lastly, we refit the individual transit light curves with the limb-darkening parameters fixed to their optimal values as given in Table 1. The resulting light curves are shown in Figure 2, and the corresponding mid-transit times are reported in Table 4. Note that the 2022 April 2 transit was excluded from the combined light-curve fit because it was observed in a different filter; the Eastman et al. (2013) limb-darkening parameters (rather than the optimal parameters from MCMC) were used for the final light curve of this transit.

Table 1. Median posterior values of impact parameter b, scaled stellar radius R_*/a , planet-to-star radius ratio R_p/R_* , and limb-darkening coefficients u_1 and u_2 derived from MCMC fit on stacked light curve. The third column lists the bounds for the uniform priors.

Parameter	Value	Prior	
b	$8.3^{+2.6}_{-2.7}$	(5, 9.5)	
R_*/a	$0.00294^{+0.00058}_{-0.00036}$	(0.002, 0.004)	
R_p/R_*	$8.4^{+2.5}_{-2.6}$	(5, 12)	
u_1	$0.52^{+0.32}_{-0.32}$	(0, 1)	
u_2	$0.52^{+0.34}_{-0.34}$	(0,1)	

2.4. Orbital-change models

The initial motivation for this work was to confirm or rule out secular changes in the orbital period of WD 1856 b. Detecting nonlinearities in the transit timing would provide further clues as to how the planet evolved onto such a tight orbit. For example, if interactions with another body in the system cause WD 1856 b's orbital period to vary over time, then it would be plausible that the same body was also responsible for kicking WD 1856 b onto its present orbit. Alvarado et al. (2024) presented two new transit observations of WD 1856 b which are marginally better explained by a *growing* orbit than by a constant-period model. We aim to improve upon their results by extending the transit-timing baseline over an additional 800 orbital cycles.

For this analysis we combined our 20 Nickel observations, described above, with 48 transits recorded in the literature (see Table 4). We used emcee to fit a constant-period model and an orbital-decay/growth model to the transit-timing observations (Foreman-Mackey et al. 2013). The constant-period model is described by

$$t(E) = t_0 + PE, \tag{1}$$

where t_0 denotes the reference transit, P the period, and E the epoch (orbital cycle) number. The orbital-decay/growth model has the same form, but with an extra term to account for the rate of change of orbital period:

$$t(E) = t_0 + PE + \frac{1}{2} \frac{dP}{dE} E^2.$$
 (2)

Here t_0 , P, and dP/dE are treated as free parameters in the MCMC fits and are initialized with wide uniform priors. The best-fit values of these parameters for both the constant-period and orbital-growth models are reported in Table 2. Based on our best-fit value

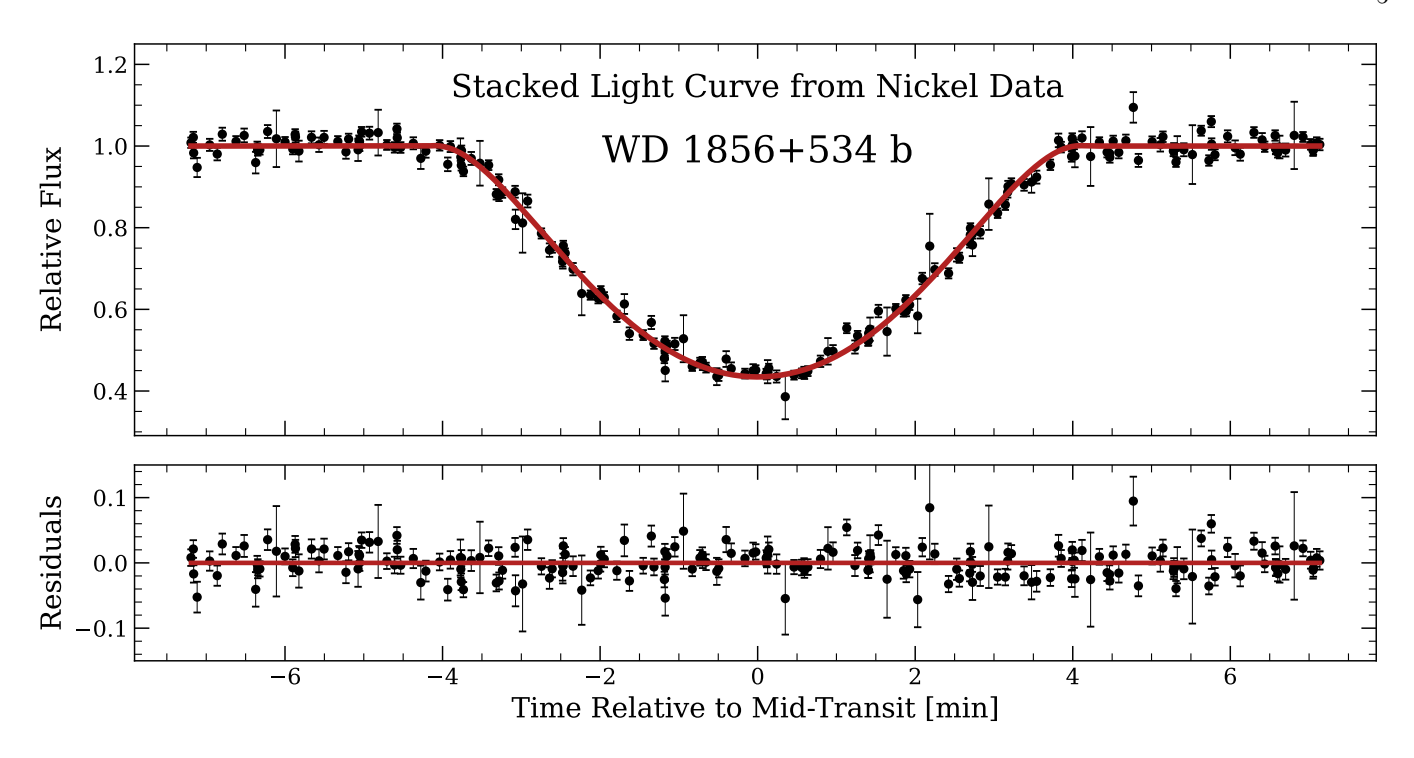


Figure 1. Stacked light curve of WD 1856+534 b generated from data obtained for this work.

Table 2. Best-fit values of reference transit t_0 , orbital period P, and period growth rate dP/dE obtained using emcee under constant-period and orbital-growth models.

Parameter	Constant Period	Orbital Growth
t_0 (days)	$2458779.375083 \pm 10^{-6}$	$2459204.572725 \pm 10^{-6}$
P (days)	$1.407939211 \pm (5 \times 10^{-9})$	$1.407939212 \pm (7 \times 10^{-9})$
$\frac{dP}{dE} \left(\frac{\text{days}}{\text{epoch}} \right)$	_	$(0.2 \pm 1.9) \times 10^{-11}$

of $dP/dE = (0.2 \pm 1.9) \times 10^{-11}$, we use

$$\dot{P} = \frac{1}{P} \frac{dP}{dE} \tag{3}$$

to estimate the time derivative of the period as $\dot{P}=0.04\pm0.43~\rm ms~yr^{-1}$. Because our best-fit value of \dot{P} is consistent with zero, we do not find any evidence of orbital growth or decay in this system. However, our results can be used to place constraints on the tidal quality factor of the system.

3. RESULTS

3.1. Constraints on modified stellar tidal quality factor

The modified stellar tidal quality factor Q'_* describes the overall efficiency of tidal dissipation inside a star, incorporating the effects of its internal structure through the Love number (Ilić et al. 2024). It can be shown that Q'_* is related to the time derivative of the period \dot{P} by

$$Q_*' = \frac{27\pi}{2|\dot{P}|} \left(\frac{M_p}{M_*}\right) \left(\frac{R_*}{a}\right)^5,\tag{4}$$

where M_p is the mass of the planet, M_* is the mass of the star, R_* is the radius of the star, and a is the planet's semimajor axis (Goldreich & Soter 1966; Patra et al. 2017; Alvarado et al. 2024). Using the most negative value of \dot{P} consistent with our results in Section 2.4 to within 2σ , the stellar mass reported by Vanderburg et al. (2020), the planetary mass reported by Limbach et al. (2025), and the scaled stellar radius derived from our MCMC fits in Section 2.3, we estimate that Q'_{\star} must be no smaller than 0.0034. This is a remarkably weak limit compared to the measured $Q'_* \approx 10^5$ for the hot-Jupiter system WASP-12 b (Patra et al. 2017; Patra et al. 2020; Yee et al. 2020). The reason we are unable to constrain Q'_* effectively is that the white dwarf is extremely compact, making it difficult for the planet to raise measurable tides on the star.

3.2. Constraints on planetary tidal quality factor

Given that the cold Jupiter does not appear to raise tides on the white dwarf, we propose that the orbital evolution of the system must instead be dominated by

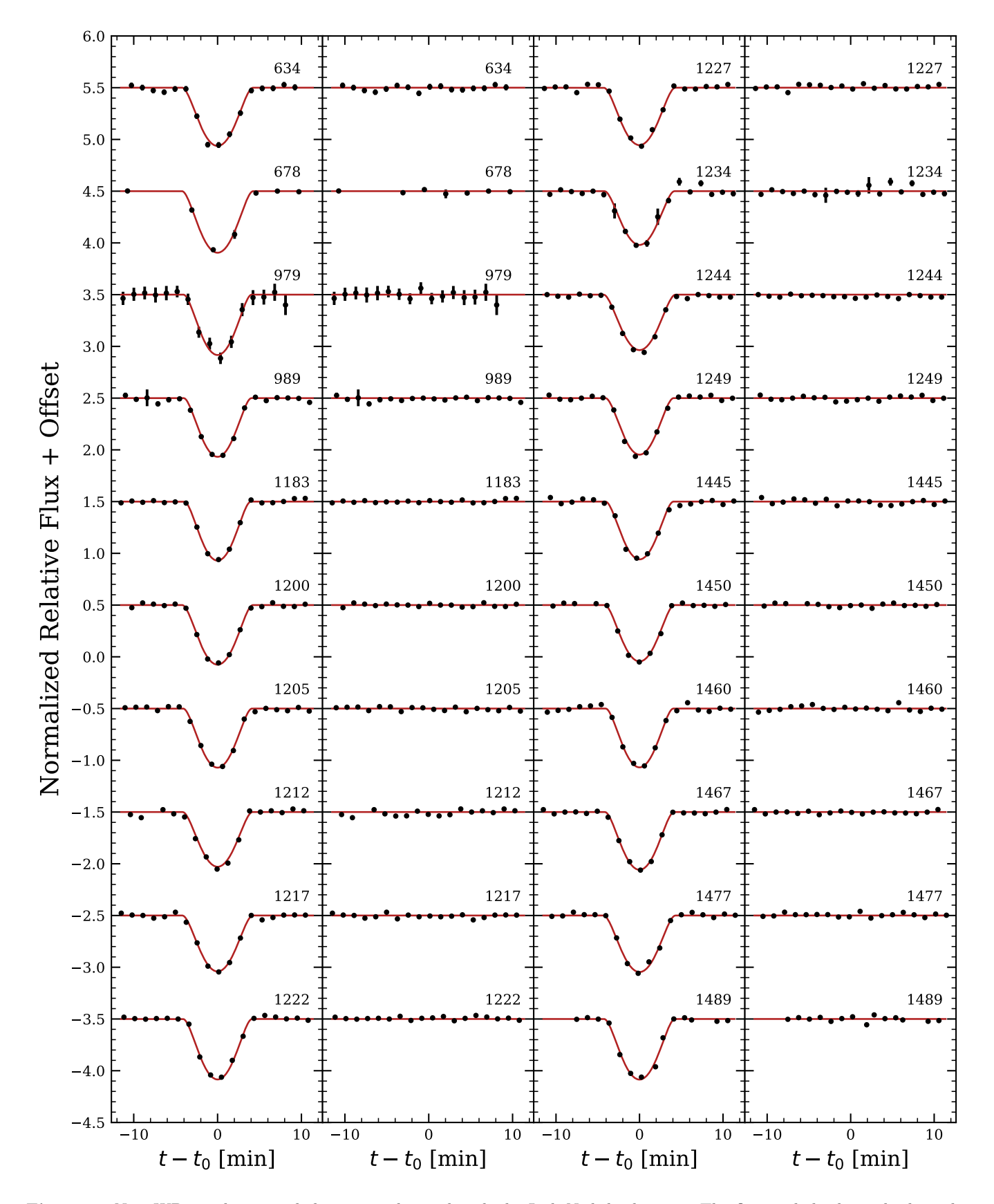


Figure 2. New WD 1856 b transit light curves obtained with the Lick Nickel telescope. The first and third panels show the data points (black) and fitted light curves (red) with epoch number labeled on the right. The second and fourth panels display the corresponding residuals. Vertical offsets were applied to separate the transits.

tides raised on the planet. The planetary tidal quality factor for a noneccentric planet in a system with no obliquity and $Q'_* = \infty$ is given by

$$Q_p' = \frac{27\pi}{|\dot{P}|} \left(\frac{M_*}{M_p}\right) \left(\frac{R_p}{a}\right)^5 \,, \tag{5}$$

where R_p denotes the planet's radius and \dot{P} , M_* , M_p , and a are as in Section 3.1 (Yang & Wei 2022). Note that Equation 5 is valid in the conservative limit where we assume the planet's rotation rate is much smaller than the mean motion (as is the case for the most tidally dissipative system). As before, we use the most negative value of \dot{P} consistent with our results in Section 2.4 to within 2σ , the stellar mass reported by Vanderburg et al. (2020), the planetary mass reported by Limbach et al. (2025), and the scaled stellar radius derived from our MCMC fits to estimate that Q_p' must be no smaller than 3.1×10^6 . This value is comparable to the planetary tidal quality factor of Jupiter in our own Solar System, which is estimated to be between 10^5 and 10^6 (Wu 2005).

Our result implies that any observed transit-timing variations should be attributed to tides raised on the planet rather than on the star. In order for planetary tides to affect orbital evolution, the planet must *not* be locked in spin-orbit synchronization with its host star, because tidal dissipation on the planet would cease once the system becomes tidally locked. Most close-in giant planets are believed to be tidally locked because the timescales for spin-orbit synchronization of close-in planets are very short compared to the stellar main-sequence lifetimes (Guillot et al. 1996; Jackson et al. 2008; Showman et al. 2015). In particular, the time for a planet's rotation period to slow down to its orbital period can be approximated as

$$\tau \approx Q_p' \left(\frac{\omega_p R_p^3}{GM_p}\right) \left(\frac{M_p}{M_*}\right)^2 \left(\frac{a}{R_p}\right)^6,$$
 (6)

where ω_p denotes the planet's primordial rotation speed (Showman et al. 2015; Guillot et al. 1996). Adopting the minimum value of Q_p' derived above and $\omega_p \approx 1.7 \times 10^{-4} \ {\rm s}^{-1}$ (same as for Jupiter in our own Solar System) yields a tidal synchronization timescale of at least $\tau \approx 4.4$ Myr. Given that planetary systems evolve on timescales of billions of years, it would be a remarkable coincidence to observe WD 1856+534 b within the few million years before it reached spin-orbit synchronization. Thus, the implication here is that either the planet is already tidally locked with the star or Q_p' is actually much larger, $Q_p' \gtrsim 10^9$. Regardless, our conservative limit of $Q_p' \gtrsim 10^6$ holds true.

3.3. Constraints on additional planets from TTVs

To place constraints on the presence of additional planets in the WD 1856 system, we compared the observed transit times to the transit times that would be expected for a variety of hypothetical companion planets. Our analysis is inspired by that of Kubiak et al. (2023), who use a 431 day baseline of transit-timing observations to rule out the presence of a companion larger than $2 M_{\rm J}$ with an orbital period less than 500 days. Following Kubiak et al. (2023), we used the TTVFast code to efficiently simulate the expected transit times as the physical parameters of the outer planet are varied (Deck et al. 2014).

The orbital elements and planetary masses adopted for the TTVFast simulations are summarized in Table 3. We initialized the integrator with the stellar mass equal to the sum of the WD 1856 mass reported by Vanderburg et al. (2020) (0.518 M_{\odot}) and the planetary mass reported by Limbach et al. (2025) $(5.2 M_J)$. Note that it is important to include WD 1856 b's mass in the stellar mass because TTVFast assumes the planetary masses are negligible when computing the companion's orbital period, but in this system the planet-to-star mass ratio is around 1% (Kubiak et al. 2023). We set WD 1856 b's period and reference transit to the values obtained by fitting a linear model to our observed transit times (see Section 2.4). We also assumed a circular orbit for WD 1856 b and adopted the inclination of 88.778° reported by Vanderburg et al. (2020).

We began by studying hypothetical companions with masses between $\sim 1\,M_{\oplus}$ and $\sim 13\,M_{J}$ and periods between 50 days and 1500 days. Given that exploring a seven-dimensional parameter space with a grid search would be prohibitively expensive, we chose to focus on companions with circular orbits coplanar to that of WD 1856 b; that is, the companion's inclination and longitude of ascending node (LAN) are fixed to those of WD 1856 b. In addition, we initialized the argument of periastron (which has no physical meaning for circular orbits) to 0 and allowed the mean anomaly of the companion to vary over all possible values.

We constructed a $300\times100\times100$ grid of evenly spaced points between the minimum and maximum values of the companion mass, period, and mean anomaly listed in Table 3. At each point in the grid, we computed the expected transit times for a system consisting of the star WD 1856, the cold Jupiter WD 1856 b, and the hypothetical companion planet. We integrated over $2092\,\mathrm{days}$ —long enough to cover the baseline of our observations— with a $0.02\,\mathrm{day}$ time-step. We then added a small correction factor to account for the Rømer delay, which is neglected in the TTVFast simulations but can

become significant in systems with a short-period inner planet and a long-period outer planet (Kubiak et al. 2023; Rappaport et al. 2013). To this end, we computed the amplitude of the Rømer delay as in Rappaport et al. (2013):

$$A_{\text{Rømer}} = \left(\frac{G}{c^3 4\pi^2}\right)^{1/3} P_{\text{outer}}^{2/3} M_{\text{outer}} M_{\text{tot}}^{-2/3} \sin i$$
. (7)

Because we are assuming noneccentric orbits, the full time-dependent Rømer delay can be expressed as

$$R(t) \approx A_{\text{Rømer}} \sin u(t) = A_{\text{Rømer}} \sin \left[\frac{2\pi}{P_{\text{inner}}} (t - t_0) \right],$$
(8)

where we have set the eccentric anomaly u(t) equal to the mean anomaly $M(t) = \frac{2\pi}{P_{\text{Inner}}}(t-t_0)$ (Rappaport et al. 2013). We then computed the observed and expected TTVs by fitting a linear model to the transit times as a function of epoch number. Allowing the orbital period and reference transit time to vary instead of fixing them to the best-fit values ensures that our results are not biased by possible discrepancies between the true orbital period and the orbital period observed over a short baseline (Kubiak et al. 2023). From here we calculated the χ^2 test statistic by comparing the observed and expected TTVs, where the uncertainties were taken to be the standard deviations on the individual mid-transit times reported in Section 2.3.

After computing the χ^2 value at each grid point, we collapsed the grid along the mean-anomaly dimension by selecting the mean-anomaly value that yielded the lowest χ^2 for every combination of mass and period. We then defined the likelihood of each hypothetical companion as $\mathcal{L} = e^{-\chi^2/2}$ and plotted the ratio of the likelihood at each grid point to the likelihood of the constant-period model (see Figure 4). Using this method, we found that the most probable hypothetical outer planet has a mass of $3.61\,M_J$ and a period of $255\,\mathrm{days}$. The χ^2 test statistic for this model is 95.68, slightly smaller than the constant-period $\chi^2 = 103.3$.

To improve our resolution in the most probable region of phase space, we repeated the analysis on another $300 \times 100 \times 100$ grid with the maximum companion mass set to $4\,M_J$ and the maximum companion period set to 400 days. We also adopted a logarithmic scale for the spacing between grid points along the period dimension to more thoroughly explore the short-period region. This time the minimum χ^2 value of 91.81 occurred with a companion mass of 0.939 M_J and a companion period of 99.5 days (see Figure 5). We plotted the TTVs for this optimal companion as well as the constant-period model in Figure 6. Given that the improvement in the

 χ^2 test statistic is relatively small, we do not find any evidence for additional planets in the WD 1856 system.

To quantify this conclusion, we computed the Bayesian information criterion (BIC) for each model evaluated in the grid search. The BIC is a statistical metric designed to compare models based on both goodness of fit and model complexity (Schwarz 1978). The BIC is defined by

$$BIC = k \ln n - 2 \ln \mathcal{L}, \tag{9}$$

where k is the number of free parameters in the model, n is the number of transit observations, and \mathcal{L} is the likelihood of the model. We ultimately found that the BIC is lower for the constant-period model than for any model including a companion planet, and that the constant-period model is preferred ($\Delta \text{BIC} > 5$) over all companion planets with masses greater than 4.1 M_J and periods < 1500 days. When only considering companion planets with periods shorter than 700 days we found that the constant-period model is preferred over all companion planets with masses greater than $2.3\,M_J$.

Given that grid search is only feasible in lowdimensional cross sections of phase space, we have also experimented with a seven-dimensional MCMC fit built on top of the TTVFast simulator. We specified wide priors on all seven parameters and included a nuisance parameter to account for possible mismodeling of the uncertainties. As for the light-curve and orbital-growth fits, we initialized 32 walkers in a small Gaussian ball near the maximum-likelihood solution and used emcee to sample the posterior distributions. The projection of the posterior distribution onto the mass and period dimensions is shown in Figure 3. We ultimately found that the posteriors hit the prior bounds, which means we cannot infer best-fit values for the physical parameters of a hypothetical companion from our results. Moreover, the region with highest density is the low-mass, high-period region where our observations have almost no sensitivity. The lack of strong constraints on parameters other than the mass and period reinforces the grid-search results by demonstrating that there are no regions of phase space with significantly higher probability that were overlooked when selecting low-dimensional cross sections for the grid search.

4. DISCUSSION

Although we have not found evidence for orbital evolution or additional planets in the system, our results nonetheless have implications for the formation history of this system. First, we look at common-envelope (CE) evolution

A CE origin for WD 1856 b is energetically not favored. In the standard α -formalism, envelope ejection

Parameter	$\rm WD1856b$	Companion Min.	Companion Max.
Mass (M_J)	0	0.003	13
Period (days)	1.4079392	50	1500
Eccentricity	0	0	0
Inclination	88.778°	88.778°	88.778°
LAN	0°	0°	0°
Arg. periastron	0	0	0
Mean anomaly	0°	0°	360°

Table 3. Orbital elements and planetary masses used to compute expected transit times with TTVFast.

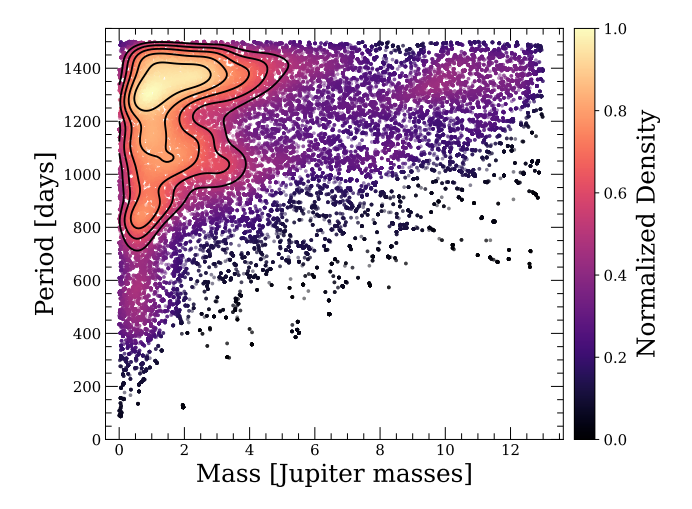


Figure 3. Two-dimensional projection of posterior distribution sampled by emcee when fitting the TTVFast transit—timing model to the observed transit times. The probability distribution function used to color points and compute contours was smoothed using Gaussian Kernel Density Estimation. The lighter colors denote regions of higher probability density. Contours are drawn at 50%, 60%, 70%, 80%, and 90% of the peak probability density.

requires $\alpha_{\rm CE} \Delta E_{\rm orb} \gtrsim E_{\rm bind}$, where $E_{\rm bind}$ is the binding energy of the red giant's envelope and $\Delta E_{\rm orb}$ is the orbital energy released by the planet during inspiral (Ivanova et al. 2013). For a typical $1\,M_\odot$ red-giant progenitor with a $0.6\,M_\odot$ core, a radius of $R_*\approx 100\,R_\odot$, and an envelope mass $M_{\rm env}\approx 0.4\,M_\odot$, the envelope binding energy is $E_{\rm bind}\approx 3\times 10^{46}\,{\rm erg}$. By contrast, a $5.2\,M_{\rm J}$ planet spiraling in from large separation to the currently observed $a_f=0.02\,{\rm AU}$ releases only $\Delta E_{\rm orb}\approx GM_{\rm core}M_p/(2a_f)\approx 1\times 10^{45}\,{\rm erg}$, more than an order of magnitude too small to unbind the envelope. This would require an unphysical efficiency $\alpha_{\rm CE}\approx 25$. Thus, WD 1856 b could not have reached its present orbit through CE evolution and must have migrated inward through a different mechanism (e.g., HETM).

A planet with a nonzero eccentricity and tidal deformation is expected to undergo apsidal precession at a rate given by

$$\frac{d\omega}{dE} = 15\pi k_p \left(\frac{M_*}{M_p}\right) \left(\frac{R_p}{a}\right)^5 \tag{10}$$

(Ragozzine & Wolf 2009). For the WD 1856 system, the expected apsidal precession rate of the planet's orbit is $d\omega/dE=2.55\times 10^{-5}\,\mathrm{rad}$ epoch⁻¹, assuming a Jupiter-like Love number $k_p=0.565$ (Durante et al. 2020). At this precession rate, the argument of periastron advances by $\Delta\omega\simeq d\omega/dE\times E\simeq 2.55\times 10^{-5}\times 1500\,\mathrm{rad}\approx 3.8\times 10^{-2}\,\mathrm{rad}$ over the 1500 observed orbits. Thus the current observation baseline samples a minuscule fraction of the precession cycle.

For a slowly precessing, mildly eccentric orbit, the characteristic amplitude of the precession-induced TTV signal is of order $A_{\rm TTV} \approx (eP/2\pi)\,\Delta\omega$, which for $P=1.4~{\rm d}~(\approx 1.21\times 10^5~{\rm s})$ gives $A_{\rm TTV} \approx e\times 7.4\times 10^2~{\rm s}$. Thus an eccentricity e=0.01 would produce a coherent TTV signal with amplitude $\sim 7-8~{\rm s}$ across the dataset, while e=0.001 would correspond to a sub-second signal. The combined O-C diagram in Figure 6 shows no evidence for coherent curvature or sinusoidal structure at amplitudes $\gtrsim 5~{\rm s}$ over 1500 epochs. Adopting this as a conservative detection threshold implies $e|\cos\omega|\lesssim 7\times 10^{-3}$; marginalizing over a uniform prior in ω then yields a robust upper limit of $e\lesssim 10^{-2}$ from the non-detection of TTVs.

This upper limit on orbital eccentricity is also consistent with an MCMC fit. An apsidally precessing orbit causes the transit times to vary according to

$$t(E) = t_0 + P_s E - \frac{eP_a}{\pi} \cos \omega , \qquad (11)$$

where E is the epoch number, t_0 is the reference transit, P_s is the sidereal period, e is the eccentricity, P_a is the anomalistic period, and ω is the argument of pericenter $\omega(E) = \omega_0 + (d\omega/dE) E$ (Patra et al. 2017; Ragozzine & Wolf 2009). The sidereal and anomalistic periods are related to each other by

$$P_s = P_a \left(1 - \frac{1}{2\pi} \frac{d\omega}{dE} \right) . \tag{12}$$

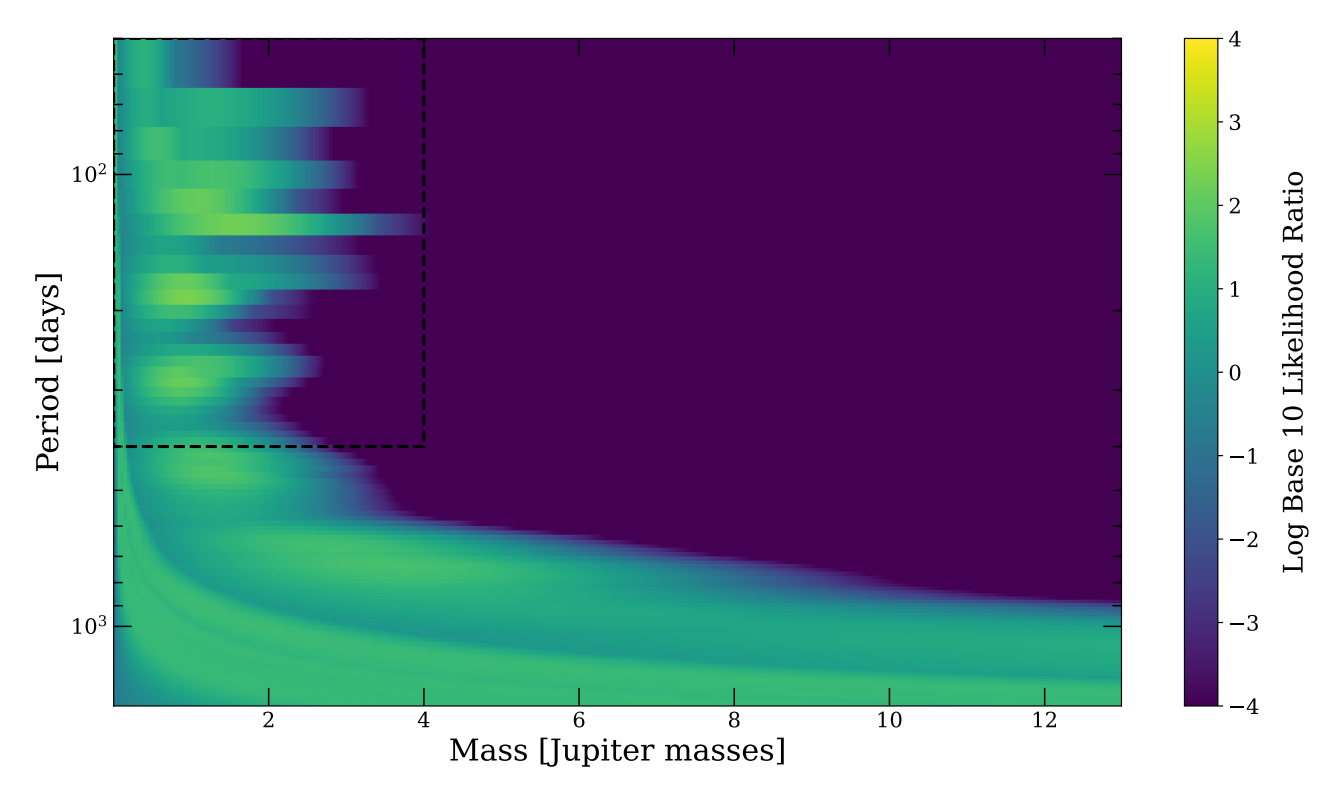


Figure 4. Log (base 10) likelihood ratio comparing hypothetical companion at 300 mass points and 100 period points to the constant-period model. Companion planets in the purple regions of phase space are incompatible with our data. The region outlined in a dashed box is explored further in Figure 5.

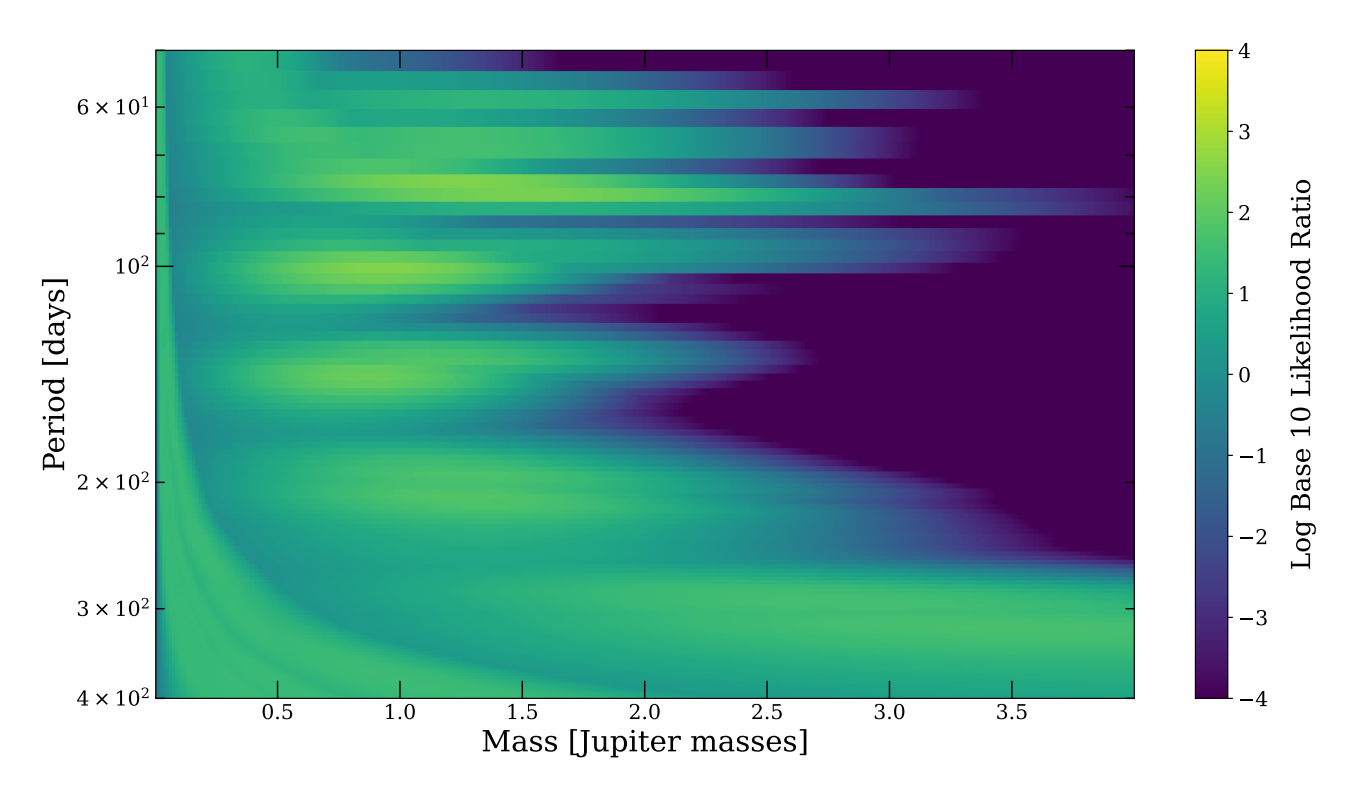


Figure 5. Log (base 10) likelihood ratio comparing hypothetical companion at 300 mass points and 100 period points to the constant-period model. This plot zooms in on the region outlined by a dashed box in Figure 4.

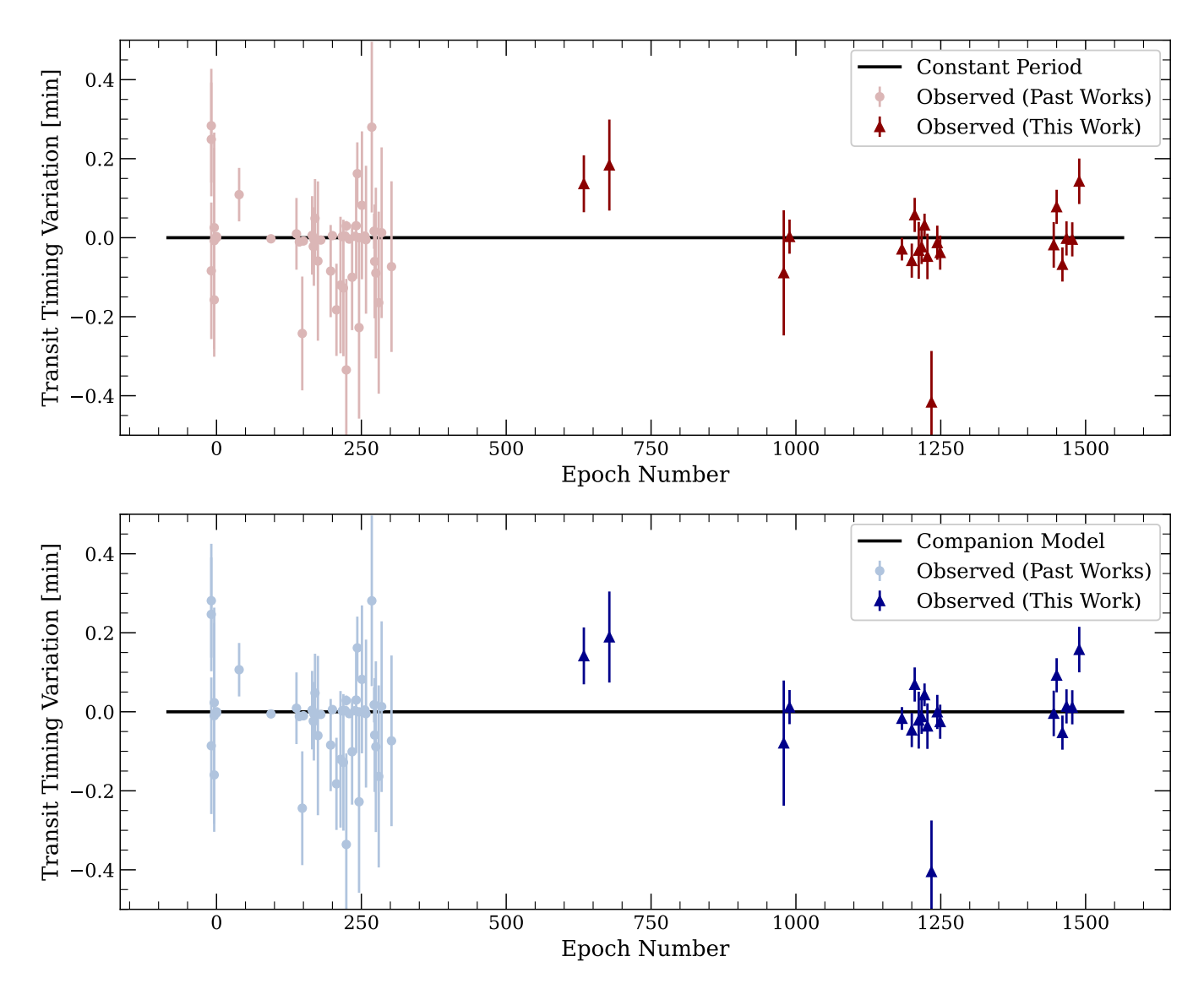


Figure 6. Transit timing variations between observed mid-transit times reported in Table 4 and expected mid-transit times. In the top panel, the expected mid-transit times are computed by fitting a linear (i.e., constant-period) model to the observed transit times. In the bottom panel, the expected mid-transit times are obtained from the TTVFast simulations assuming a coplanar $0.939 \, M_J$ companion on a circular orbit with a $99.5 \, \text{day}$ period. Note that there is no significant difference between the timing residuals, which implies that adding a companion planet to the system is not necessary to explain the observed data.

We implemented an MCMC fit with t_0 , P_s , e, ω_0 , and $d\omega/dE$ as free parameters and found that the e=0 scenario is strongly preferred, in which case both ω_0 and $d\omega/dE$ are undefined. Such a low present-day eccentricity indicates that HETM is no longer operating in this system.

The rate of tidal energy deposition into the planet is related to the planetary tidal quality factor Q'_p and the orbital eccentricity e by

$$\frac{dE}{dt} = \frac{21}{2} \frac{k_p}{Q_p'} \frac{GM_*^2 n R_p^5 e^2}{a^6} \,, \tag{13}$$

where k_p is the planet's potential Love number, M_* is the star's mass, R_p is the planet's radius, $n \approx$ $(GM_*/a^3)^{1/2}$ is the orbital mean motion, and a is the orbital semimajor axis (Peale & Cassen 1978; Peale et al. 1979; Wisdom 2004, 2008). Inserting the lower bound on Q'_p of 3.1×10^6 and the upper bound on e of 10^{-2} into Equation 13 reveals that dE/dt must be no larger than $2 \times 10^{25} \text{ erg s}^{-1}$. Limbach et al. (2025) measure the planet's effective temperature as $184 \pm 8 \,\mathrm{K}$, which implies a luminosity of roughly 4×10^{25} erg s⁻¹. Although these values are comparable, our estimate of the tidal heating rate is intentionally conservative: adopting a larger Q'_p or, especially, a smaller eccentricity would further reduce the expected tidal power. Thus it is unlikely the observed luminosity of the planet is primarily driven by tidal heating of the planet. This again implies that if the Kozai-Lidov process took place in this system's past, it must have already concluded.

5. CONCLUSIONS

In this work, we have analyzed transit observations of WD 1856 b to place constraints on the presence of orbital evolution and additional planets in the system. The WD 1856 system offers a unique opportunity to probe planetary-migration hypotheses because the planet orbits too close to its host star to have survived the host star's red-giant phase at its present location. Commonenvelope evolution has been proposed to explain the short semimajor axis without invoking planetary migration, but recent measurements placing the planet's mass below $6 M_I$ make that explanation improbable. Higheccentricity tidal migration offers a more natural explanation for the observed semimajor axis — but only if we posit the existence of a perturber responsible for exciting the cold Jupiter onto a highly eccentric orbit in the first place. There are many candidates for such a perturber including companion planet(s), a stellar flyby, or the Mdwarfs G229-20A/B, which are gravitationally bound to WD 1856. Here we have focused on the easiest perturber to detect: an additional planet in the WD 1856 system.

We compiled 48 observations of WD 1856 b transits from the literature and 20 new transits from our observations with the Lick Nickel telescope, 18 of which were previously unpublished. The Nickel data extend the transit-timing baseline from 311 epochs to 1498 epochs, significantly improving our ability to detect transit-timing variations due to companion planets. We used this dataset to investigate early evidence of orbital growth reported by Alvarado et al. (2024) and ultimately found no evidence for a changing period over a longer baseline. We also explored whether the observed transit-timing variations are consistent with additional planets of various masses and periods using both grid search and MCMC methods. The lack of evidence for any companion planet further complicates the question of how this planetary system formed, because the most plausible formation hypothesis still requires that we invoke an unseen perturber. It is important to note that while our data allow us to rule out a large close-in planet as the perturber, we cannot yet rule out smaller close-in planets and larger planets at greater distances.

We believe tidal migration remains a plausible explanation for WD 1856 b's present semimajor axis, but the chances of detecting the perturber appear to be diminishing. It is not possible to confirm or rule out the possibility of a stellar flyby, and we are unlikely to find a companion planet if it was ejected from the system in the course of the interaction that excited WD 1856 b onto an eccentric orbit. That being said, uncovering the formation history of the WD 1856 system would greatly advance our understanding of planetary migration, which justifies continued transit timing observations over an extended baseline. Our 2σ upper limit on the period derivative of 0.9 ms yr⁻¹ indicates the planetary tidal quality factor is no smaller than 3.1×10^6 . Based on the lack of observed TTVs, we determined that the maximum possible eccentricity is 10^{-2} . If HETM is responsible for bringing the cold Jupiter to its present 0.02 AU orbital distance, then the process has already run its course and left the planet on a nearly circularized orbit. Altogether, we hope that our new transit observations, combined with the nondetections of orbital growth and of additional planets, will contribute to ongoing efforts to understand the formation history of the unique WD 1856 system.

ACKNOWLEDGMENTS

We thank UC Berkeley undergraduate students Gracelynn Jost and Arnav Swaroop, who assisted with transit observations while training on the Nickel telescope. Re-

search at Lick Observatory is partially supported by a gift from Google.

A.V.F.'s research group at UC Berkeley received financial assistance from the Christopher R. Redlich Fund, as well as donations from Gary and Cynthia Bengier, Clark and Sharon Winslow, Alan Eustace and Kathy Kwan, William Draper, Timothy and Melissa Draper, Briggs and Kathleen Wood, Sanford Robertson (W.Z. is a Bengier-Winslow-Eustace Specialist in

Astronomy, T.G.B. is a Draper-Wood-Robertson Specialist in Astronomy), and numerous other donors.

DATA AVAILABILITY

The raw Nickel data from 2022 and 2023 are publicly available on the Mount Hamilton Data Repository.⁵ The 2024 and 2025 data will become public at the same link approximately 2 yr after the observation date. The analysis code is available at https://github.com/eligd/wd-1856-534b.

APPENDIX

A. MID-TRANSIT TIMES

Here we present the mid-transit times for the WD 1856 system from the literature and this work. The 20 new data points increase the total number of observations to 68 and extend the transit-timing baseline from 311 epochs to 1498 epochs.

REFERENCES

- Alonso, R., Rodríguez-Gil, P., Izquierdo, P., et al. 2021, Astronomy & Astrophysics, 649, A131, doi: 10.1051/0004-6361/202140359
- Alvarado, III, E., Bostow, K. B., Patra, K. C., et al. 2024, Monthly Notices of the Royal Astronomical Society, 534, 800–813, doi: 10.1093/mnras/stae2062
- Barber, S. D., Patterson, A. J., Kilic, M., et al. 2012, The Astrophysical Journal, 760, 26, doi: 10.1088/0004-637x/760/1/26
- Becker, J., Seligman, D. Z., Adams, F. C., & Styczinski, M. J. 2023, The Astrophysical Journal Letters, 945, L24, doi: 10.3847/2041-8213/acbe44
- Blackman, J. W., Beaulieu, J. P., Bennett, D. P., et al. 2021, Nature, 598, 272–275, doi: 10.1038/s41586-021-03869-6
- Blouin, S., Allard, N. F., Leininger, T., Gadéa, F. X., & Dufour, P. 2019, The Astrophysical Journal, 875, 137, doi: 10.3847/1538-4357/ab1266
- Brinkworth, C. S., Gänsicke, B. T., Girven, J. M., et al. 2012, The Astrophysical Journal, 750, 86, doi: 10.1088/0004-637x/750/1/86
- Brinkworth, C. S., Gänsicke, B. T., Marsh, T. R., Hoard,
 D. W., & Tappert, C. 2009, The Astrophysical Journal,
 696, 1402–1406, doi: 10.1088/0004-637x/696/2/1402
- Burkart, J., Quataert, E., Arras, P., & Weinberg, N. N. 2013, Monthly Notices of the Royal Astronomical Society, 433, 332–352, doi: 10.1093/mnras/stt726
- ⁵ https://mthamilton.ucolick.org/data/

- Chamandy, L., Blackman, E. G., Nordhaus, J., & Wilson, E. 2021, Monthly Notices of the Royal Astronomical Society: Letters, 502, L110–L114, doi: 10.1093/mnrasl/slab017
- Collins, K. A., Kielkopf, J. F., Stassun, K. G., & Hessman, F. V. 2017, The Astronomical Journal, 153, 77, doi: 10.3847/1538-3881/153/2/77
- Dawson, R. I., & Johnson, J. A. 2018, Annual Review of Astronomy and Astrophysics, 56, 175–221, doi: 10.1146/annurev-astro-081817-051853
- De, K., MacLeod, M., Karambelkar, V., et al. 2023, Nature, 617, 55, doi: 10.1038/s41586-023-05842-x
- Debes, J. H., Walsh, K. J., & Stark, C. 2012, The Astrophysical Journal, 747, 148, doi: 10.1088/0004-637x/747/2/148
- Deck, K. M., Agol, E., Holman, M. J., & Nesvorný, D. 2014, The Astrophysical Journal, 787, 132, doi: 10.1088/0004-637x/787/2/132
- Durante, D., Parisi, M., Serra, D., et al. 2020,Geophys. Res. Lett., 47, e86572,doi: 10.1029/2019GL086572
- Eastman, J., Gaudi, B. S., & Agol, E. 2013, Publications of the Astronomical Society of the Pacific, 125, 83–112, doi: 10.1086/669497
- Efroimsky, M., & Makarov, V. V. 2022, Universe, 8, 211, doi: 10.3390/universe8040211
- Farihi, J., Parsons, S. G., & Gänsicke, B. T. 2016, A Circumbinary Debris Disk in a Polluted White Dwarf System. https://arxiv.org/abs/1612.05259

Table 4. Mid-transit times for the WD 1856 system.

LITC Data	Enoch	T (PID days)	$1\sigma (10^{-5} \text{ days})$	Sauraa
UTC Date 2019 Oct. 10	Epoch -9	$T_{\text{mid}} \text{ (BJD}_{\text{TDB}}, \text{ days)}$ 2458766.703572	10 (10 days)	Source Vanderburg et al. (2020)
2019 Oct. 10	-9	2458766.703803	10	Vanderburg et al. (2020)
2019 Oct. 10	-9	2458766.703827	10	Vanderburg et al. (2020)
2019 Oct. 17	-4	2458773.743217	10	Vanderburg et al. (2020)
2019 Oct. 17	-4	2458773.743321	19	Vanderburg et al. (2020)
2019 Oct. 17	-4	2458773.743344	14	Vanderburg et al. (2020)
2019 Oct. 23 2019 Oct. 23	0	2458779.375085	0.20	Vanderburg et al. (2020)
2019 Oct. 23 2019 Dec. 17	0 39	2458779.375083 2458834.284788	$0.34 \\ 4.7$	Mallonn (2020) Vanderburg et al. (2020)
2020 Mar. 3	94	2458911.721367	0.30	Alonso et al. (2021)
2020 May 4	138	2458973.670701	6.3	Alonso et al. (2021)
2020 May 11	143	2458980.710383	0.80	Alonso et al. (2021)
$2020~\mathrm{May}~18$	148	2458987.749918	10	Kubiak et al. (2023)
$2020~\mathrm{May}~21$	150	2458990.565959	0.60	Alonso et al. (2021)
2020 June 11	165	2459011.685057	6.9	Kubiak et al. (2023)
2020 June 14	167	2459014.500916	0.70	Alonso et al. (2021)
2020 June 15 2020 June 15	168	2459015.908855	6.9	Kubiak et al. (2023)
2020 June 15 2020 June 15	168 168	2459015.908868 2459015.908869	$0.21 \\ 0.22$	Xu et al. (2021) Xu et al. (2021)
2020 June 18	170	2459018.724783	6.9	Kubiak et al. (2023)
2020 June 25	175	2459025.764404	14	Kubiak et al. (2023)
2020 July 2	180	2459032.804137	0.22	Xu et al. (2021)
2020 July 26	197	2459056.739049	8.1	Kubiak et al. (2023)
$2020~\mathrm{July}~30$	200	2459060.962929	0.18	Xu et al. (2021)
2020 Aug. 9	207	2459070.818373	8.1	Kubiak et al. (2023)
2020 Aug. 19	214	2459080.673991	12	Kubiak et al. (2023)
2020 Aug. 23	217	2459084.897894	0.24	Xu et al. (2021)
2020 Aug. 26 2020 Aug. 30	$\frac{219}{222}$	2459087.713682 2459091.937591	12 0.33	Kubiak et al. (2023)
2020 Aug. 30 2020 Sept. 2	224	2459091.937391	16	Xu et al. (2021) Kubiak et al. (2023)
2020 Sept. 2	224	2459094.753487	0.87	Xu et al. (2021)
2020 Sept. 9	229	2459101.793160	0.18	Xu et al. (2021)
2020 Sept. 16	234	2459108.832789	9.3	Kubiak et al. (2023)
$2020~\mathrm{Sept.}$ 23	239	2459115.872557	0.25	Xu et al. (2021)
2020 Sept. 26	241	2459118.688454	9.3	Kubiak et al. (2023)
2020 Sept. 29	243	2459121.504424	5.5	Mallonn (2020)
2020 Oct. 3 2020 Oct. 3	$\frac{246}{246}$	2459125.727971 2459125.728129	16	Kubiak et al. (2023) Xu et al. (2021)
2020 Oct. 3 2020 Oct. 10	251	2459123.767882	0.25 13	Kubiak et al. (2023)
2020 Oct. 17	256	2459139.807524	0.28	Xu et al. (2021)
2020 Oct. 20	258	2459142.623396	13	Kubiak et al. (2023)
2020 Nov. 3	268	2459156.702986	15	Kubiak et al. (2023)
2020 Nov. 9	272	2459162.334560	3.1	Mallonn (2020)
2020 Nov. 10	273	2459163.742446	10	Kubiak et al. (2023)
2020 Nov. 13	275	2459166.558304	15	Kubiak et al. (2023)
2020 Nov. 20	280	2459173.597948	16	Kubiak et al. (2023)
2020 Nov. 27 2020 Dec. 21	$\frac{285}{302}$	2459180.637767 2459204.572674	15 15	Kubiak et al. (2023)
2022 Apr. 2	634	2459672.008638	5.0	Kubiak et al. (2023) This work
2022 June 3	678	2459733.957996	8.0	This work
2023 Aug. 1	979	2460157.747509	11	This work
2023 Aug. 15	989	2460171.826965	3.0	This work
$2024~\mathrm{May}~14$	1183	2460444.967150	2.0	This work
2024 June 7	1200	2460468.902096	3.0	This work
2024 June 14	1205	2460475.941873	3.0	This work
2024 June 24	1212	2460485.797385	5.0	This work
2024 July 1 2024 July 8	1217	2460492.837087	3.0	This work This work
2024 July 8 2024 July 15	1222 1227	2460499.876821 2460506.916462	$\frac{2.0}{4.0}$	This work This work
2024 July 15 2024 July 25	1234	2460506.916462	9.0	This work This work
2024 July 25 2024 Aug. 8	1244	2460530.851453	3.0	This work
2024 Aug. 15	1249	2460537.891132	3.0	This work
2025 May 18	1445	2460813.847231	4.0	This work
$2025~\mathrm{May}~25$	1450	2460820.886993	3.0	This work
2025 June 8	1460	2460834.966284	3.0	This work
2025 June 18	1467	2460844.821905	3.0	This work
2025 July 2	1477	2460858.901295	3.0	This work
2025 July 19	1489	2460875.796668	4.0	This work

- Fellay, L., Pezzotti, C., Buldgen, G., Eggenberger, P., & Bolmont, E. 2023, Astronomy & Astrophysics, 669, A2, doi: 10.1051/0004-6361/202243621
- Foreman-Mackey, D., Hogg, D. W., Lang, D., & Goodman, J. 2013, Publications of the Astronomical Society of the Pacific, 125, 306, doi: 10.1086/670067
- Goldreich, P., & Soter, S. 1966, Icarus, 5, 375, doi: 10.1016/0019-1035(66)90051-0
- Guillot, T., Burrows, A., Hubbard, W. B., Lunine, J. I., & Saumon, D. 1996, ApJL, 459, L35, doi: 10.1086/309935
- Gänsicke, B. T., Marsh, T. R., Southworth, J., &
 Rebassa-Mansergas, A. 2006, Science, 314, 1908–1910,
 doi: 10.1126/science.1135033
- Gänsicke, B. T., Schreiber, M. R., Toloza, O., et al. 2019, Nature, 576, 61–64, doi: 10.1038/s41586-019-1789-8
- Hartmann, S., Nagel, T., Rauch, T., & Werner, K. 2016, Astronomy & Astrophysics, 593, A67, doi: 10.1051/0004-6361/201628403
- Hollands, M. A., Koester, D., Alekseev, V., Herbert, E. L., & Gänsicke, B. T. 2017, Monthly Notices of the Royal Astronomical Society, 467, 4970–5000, doi: 10.1093/mnras/stx250
- Ilić, N., Poppenhaeger, K., Queiroz, A. B., & Chiappini, C. 2024, Constraining stellar tidal quality factors from planet-induced stellar spin-up. https://arxiv.org/abs/2404.04047
- Ivanova, N., Justham, S., & Ricker, P. 2020, Common Envelope Evolution, 2514-3433 (IOP Publishing), doi: 10.1088/2514-3433/abb6f0
- Ivanova, N., Justham, S., Chen, X., et al. 2013, A&A Rv, 21, 59, doi: 10.1007/s00159-013-0059-2
- Jackson, B., Greenberg, R., & Barnes, R. 2008, The Astrophysical Journal, 678, 1396–1406, doi: 10.1086/529187
- Kaltenegger, L., MacDonald, R. J., Kozakis, T., et al. 2020, The Astrophysical Journal Letters, 901, L1, doi: 10.3847/2041-8213/aba9d3
- Kilic, M., Patterson, A. J., Barber, S., Leggett, S. K., & Dufour, P. 2012, Monthly Notices of the Royal Astronomical Society: Letters, 419, L59–L63, doi: 10.1111/j.1745-3933.2011.01177.x
- Kilic, M., & Redfield, S. 2007, The Astrophysical Journal, 660, 641–650, doi: 10.1086/513008
- Kilic, M., von Hippel, T., Leggett, S. K., & Winget, D. E. 2005, The Astrophysical Journal, 632, L115–L118, doi: 10.1086/497825
- —. 2006, The Astrophysical Journal, 646, 474–479, doi: 10.1086/504682

- Koester, D., Gänsicke, B., Girven, J., & Farihi, J. 2012, Search for Metal Pollution in 81 DA White Dwarfs. https://arxiv.org/abs/1209.6036
- Koester, D., Gänsicke, B. T., & Farihi, J. 2014, Astronomy & Astrophysics, 566, A34, doi: 10.1051/0004-6361/201423691
- Kozai, Y. 1962, AJ, 67, 591, doi: 10.1086/108790
- Kubiak, S., Vanderburg, A., Becker, J., et al. 2023, Monthly Notices of the Royal Astronomical Society, 521, 4679–4694, doi: 10.1093/mnras/stad766
- Lagos, F., Schreiber, M. R., Zorotovic, M., et al. 2020, Monthly Notices of the Royal Astronomical Society, 501, 676–682, doi: 10.1093/mnras/staa3703
- Lidov, M. L. 1962, Planetary and Space Science, 9, 719–759, doi: https://doi.org/10.1016/0032-0633(62)90129-0
- Limbach, M. A., Vanderburg, A., MacDonald, R. J., et al. 2025, Thermal Emission and Confirmation of the Frigid White Dwarf Exoplanet WD 1856+534b. https://arxiv.org/abs/2504.16982
- Louden, E. M., Laughlin, G. P., & Millholland, S. C. 2023, The Astrophysical Journal Letters, 958, L21, doi: 10.3847/2041-8213/ad0843
- Luhman, K. L., Burgasser, A. J., & Bochanski, J. J. 2011, The Astrophysical Journal, 730, L9, doi: 10.1088/2041-8205/730/1/19
- Maldonado, R. F., Villaver, E., Mustill, A. J., Chávez, M., & Bertone, E. 2020, Monthly Notices of the Royal Astronomical Society: Letters, 501, L43–L48, doi: 10.1093/mnrasl/slaa193
- Mallonn, M. 2020, Research Notes of the AAS, 4, 245, doi: 10.3847/2515-5172/abd480
- Mandel, K., & Agol, E. 2002, The Astrophysical Journal, 580, L171, doi: 10.1086/345520
- Mayor, M., & Queloz, D. 1995, Nature, 378, 355–359, doi: 10.1038/378355a0
- Merlov, A., Bear, E., & Soker, N. 2021, The Astrophysical Journal Letters, 915, L34, doi: 10.3847/2041-8213/ac0f7d
- Mullally, S. E., Debes, J., Cracraft, M., et al. 2024, JWST Directly Images Giant Planet Candidates Around Two Metal-Polluted White Dwarf Stars. https://arxiv.org/abs/2401.13153
- Mustill, A. J., & Villaver, E. 2012, The Astrophysical Journal, 761, 121, doi: 10.1088/0004-637X/761/2/121
- Muñoz, D. J., & Petrovich, C. 2020, The Astrophysical Journal Letters, 904, L3, doi: 10.3847/2041-8213/abc564
- Naoz, S. 2016, Annual Review of Astronomy and Astrophysics, 54, 441–489, doi: 10.1146/annurev-astro-081915-023315

- O'Connor, C. E., Liu, B., & Lai, D. 2020, Monthly Notices of the Royal Astronomical Society, 501, 507–514, doi: 10.1093/mnras/staa3723
- Patra, K. C., Winn, J. N., Holman, M. J., et al. 2017, The Astronomical Journal, 154, 4, doi: 10.3847/1538-3881/aa6d75
- Patra, K. C., Winn, J. N., Holman, M. J., et al. 2020, AJ, 159, 150, doi: 10.3847/1538-3881/ab7374
- Peale, S., & Cassen, P. 1978, Icarus, 36, 245, doi: https://doi.org/10.1016/0019-1035(78)90109-4
- Peale, S. J., Cassen, P., & Reynolds, R. T. 1979, Science, 203, 892
- Piro, A. L. 2011, The Astrophysical Journal, 740, L53, doi: 10.1088/2041-8205/740/2/153
- Preval, S. P., Barstow, M. A., Bainbridge, M., et al. 2019, Monthly Notices of the Royal Astronomical Society, 487, 3470–3487, doi: 10.1093/mnras/stz1506
- Raddi, R., Gänsicke, B. T., Koester, D., et al. 2015, Monthly Notices of the Royal Astronomical Society, 450, 2083–2093, doi: 10.1093/mnras/stv701
- Ragozzine, D., & Wolf, A. S. 2009, ApJ, 698, 1778, doi: 10.1088/0004-637X/698/2/1778
- Rappaport, S., Deck, K., Levine, A., et al. 2013, The Astrophysical Journal, 768, 33, doi: 10.1088/0004-637x/768/1/33
- Schwarz, G. 1978, Annals of Statistics, 6, 461
- Showman, A. P., Lewis, N. K., & Fortney, J. J. 2015, Three-dimensional Atmospheric Circulation of Warm and Hot Jupiters: Effects of Orbital Distance, Rotation Period, and Non-Synchronous Rotation. https://arxiv.org/abs/1411.4731
- Sigurdsson, S., Richer, H. B., Hansen, B. M., Stairs, I. H.,
 & Thorsett, S. E. 2003, Science, 301, 193–196,
 doi: 10.1126/science.1086326
- Stephan, A. P., Naoz, S., & Gaudi, B. S. 2021, The Astrophysical Journal, 922, 4, doi: 10.3847/1538-4357/ac22a9
- Thorsett, S. E., Arzoumanian, Z., & Taylor, J. H. 1993, ApJL, 412, L33, doi: 10.1086/186933
- Vanderburg, A., Johnson, J. A., Rappaport, S., et al. 2015, Nature, 526, 546–549, doi: 10.1038/nature15527

- Vanderburg, A., Rappaport, S. A., Xu, S., et al. 2020, Nature, 585, 363–367, doi: 10.1038/s41586-020-2713-y
- Veras, D. 2021, Planetary Systems Around White Dwarfs, Oxford University Press,
- doi: 10.1093/acrefore/9780190647926.013.238
- Villaver, E., & Livio, M. 2009, The Astrophysical Journal, 705, L81–L85, doi: 10.1088/0004-637x/705/1/181
- Virtanen, P., Gommers, R., Oliphant, T. E., et al. 2020, Nature Methods, 17, 261, doi: 10.1038/s41592-019-0686-2
- Vissapragada, S., Chontos, A., Greklek-McKeon, M., et al. 2022, The Astrophysical Journal Letters, 941, L31, doi: 10.3847/2041-8213/aca47e
- Willems, B., Deloye, C. J., & Kalogera, V. 2010, The Astrophysical Journal, 713, 239, doi: 10.1088/0004-637X/713/1/239
- Wilson, D. J., Gänsicke, B. T., Koester, D., et al. 2014, Monthly Notices of the Royal Astronomical Society, 445, 1878–1884, doi: 10.1093/mnras/stu1876
- Wisdom, J. 2004, The Astronomical Journal, 128, 484, doi: 10.1086/421360
- Wisdom, J. 2008, Icarus, 193, 637, doi: 10.1016/j.icarus.2007.09.002
- Wu, Y. 2005, The Astrophysical Journal, 635, 688–710, doi: 10.1086/497355
- Xu, S., Diamond-Lowe, H., MacDonald, R. J., et al. 2021, The Astronomical Journal, 162, 296, doi: 10.3847/1538-3881/ac2d26
- Yang, F., & Wei, X. 2022, Publications of the Astronomical Society of the Pacific, 134, 024401, doi: 10.1088/1538-3873/ac495a
- Yee, S. W., Winn, J. N., Knutson, H. A., et al. 2020, ApJL, 888, L5, doi: 10.3847/2041-8213/ab5c16
- Zhang, K., Zang, W., El-Badry, K., et al. 2024, Nature Astronomy, 8, 1575–1582, doi: 10.1038/s41550-024-02375-9
- Zuckerman, B., Melis, C., Klein, B., Koester, D., & Jura, M. 2010, The Astrophysical Journal, 722, 725–736, doi: 10.1088/0004-637x/722/1/725